ISSN 2229-5518

Effect of Hole Dynamics on the Small Signal Cross Gain Modulation in Quantum-Dot Semiconductor Optical Amplifiers

Hussein H. Warid
Department of physics, Science College, Thi-Qar University
Baghdad- Iraq
Hussein_hade@yahoo.com

Abstract

The hole dynamics in undoped quantum dots semiconductor optical amplifier (QD-SOA) is investigated using four-level rate equations model preserving charge neutrality. Simple analytical expression is derived which directly connects the cross gain modulation (XGM) response to the change of hole occupation. According to the initial conditions, the main XGM mechanism is the total carrier density depletion (TCDD). The calculated small-signal XGM response shows significant dependence on the hole occupation probability . The results indicate that for an undoped QD-SOA, the exact calculation of gain change due to hole effect leads to increase the 3-dB bandwidth of the small-signal XGM response of the SOAs.

Keywords

Quantum dot , cross gain modulation, semiconductor amplifier

1. INTRODUCTION

The future of high-speed networks depends on the ability to convert optical signals from one wavelength to another wavelength- without modifying the data content of the signal- to prevent wavelength blocking and reduce the number of frequency channels needed to operate an optical network. Optical networks provide an information transmission characterized by the highest possible bandwidth and the lowest possible susceptibility to electromagnetic interferences [1]. Nonlinearities in semiconductor optical amplifiers (SOAs) are principally caused by carrier density changes induced by the amplifier input signals. The four main types of nonlinearity are: cross gain modulation (XGM), cross phase modulation (XPM), self-phase modulation (SPM), and four-wave mixing (FWM) [2]. SOAs operational performance may be improved by using quantum-dot (QD) due to low threshold current, high material gain, high saturation output power, broad gain bandwidth, and temperature-insensitive as compared to bulk and quantum well (QW) devices [3]. Quantum-dot semiconductor optical amplifier (QD-SOA) have been intensively studied as high-speed, high-performance, cost-effective optoelectronic devices for linear amplifiers and optical networks. In the XGM method, the SOA gain is saturated by one intensity modulated input signal. Therefore, it is possible to modulate the amplifier gain with an input signal and to encode (with an inverted data) a separated CW (continuous wave) carrier at a desired optical frequency. The XGM method has the advantage of a simple structure, high conversion efficiency, wide conversion range and relative polarization independence, when compared with other SOA based methods. However, its use has been limited due to high noise figure, chirp and low extinction ratio [3]. The main disadvantages of this method are substantial phase distortions due to frequency chirping, degradation due to spontaneous emission, and a relatively low extinction ratio [4]. XGM in bulk or quantum well semiconductor optical amplifiers (QW-SOAs) has been intensively studied as one of the key mechanisms to implement all-optical wavelength converters [1]. QD-SOAs have been predicted to overcome the limitation of bulk or QW SOAs due to the ultrafast gain recovery time of spectral hole burning (SHB) [2]. The maximum operation speed and converted signal quality of the wavelength converter based on XGM are limited due to the slow gain recovery time. Coupled rate equations have been used widely to calculate the carrier dynamics and optical properties of QD-SOAs. Most published works that treat rate-equation models for these amplifiers consider only the electron dynamics. The hole dynamics is assumed to be so fast with respect to the electrons so that all the gain and spontaneous emission dynamical properties of the QDs are almost determined by the electron dynamics in conduction band. Also, for the sake of

IJSER

simplicity, it has been assumed that the conduction band wetting layer (WL) carrier population together with the continuum state (CS) population are concentrated on one energy level. The continuum state merges into the energy states of WL. The CS means that the ensemble of dense energy states in each dot which merges into the two-dimensional energy states of the wetting layer. Recently, investigation of QD amplifier performance has been carried out using four-level rate equations model (4LREM) where the CS effect are taken into account. It has been found that the carrier reservoir in the WL and CS is necessary for these amplifiers to operate with high gain, high saturation power, and ultrafast gain recovery. This is because the higher injection current allowing the WL to act as a carrier reservoir for the ES and ground state (GS) even in the saturated region. Higher injection current is necessary in order to prevent the pattern effects which are commonly used in the state-of-the-art QD-SOAs. However, in this case, the excited state (ES) and theground state are filled; thus carriers will populate the continuum states in QDs. To be more accurate, the continuum states should be included in the rate equations model.

This paper is organized as follows: in section 2, the four level rate equations model (4LREM) for QD-SOA is described and characterized. Section 3 presents the expression of the charge neutrality for the whole device . In section 4, an analytical model of the small-signal XGM conversion efficiency which takes into account the hole effect is derived. In section 5, numerical results using the XGM model based on 4LREM with hole effect are reported. Finally, the conclusions drawn from this study are listed in section 6.

2. Four-Level Rate Equations Model of QD-SOA

Theoretical models have been introduced to calculate the carrier dynamics and optical properties of QD-SOAs. These models, based on rate equations, have demonstrated good agreement with experimental data for several quantum dot structures and materials. These models are more common since they are simpler and easy to solve compared with other models. Furthermore, it is easier to interpret physical phenomena and extract data from rate equations models where in some cases a closed-form solution is obtained [5]. In these models, the carrier dynamics is determined by the relaxation of electrons in the conduction band, because of the much larger effective mass of holes and lower quantization energies of the QD levels in the valence band which results in a faster relaxation of holes. Therefore, electrons behavior limits the carrier dynamics while holes in the valence band are assumed to be in quasi-thermal equilibrium at all times. Our objective in this paper is to investigate the hole effect on the small-signal XGM conversion efficiency by using 4LREM. The QDs are assumed to have two discrete energy states, i.e., ground state (GS) and excited state (ES), and a continuum state (CS), which is an ensemble of dense excited states in each dot. Different dots are interconnected through a two-dimensional (2-D) WL. Our model ignores barrier dynamics and assumes the electrons are injected directly into the WL, then captured by the CS and finally relaxed into the ES and GS. The direct carrier capture into GS and ES is neglected due to the fast intradots carrier relaxation and the large energy separation between GS, ES and WL. The corresponding rate equations describing the change in carrier (electron) densities in the WL, CS, ES, and GS, can be written as [6]

$$\frac{\partial N_w}{\partial t} = \frac{J}{e l_w} - \frac{N_w(1-f_c)}{\tau_{wc}} + \frac{N_c(1-f_w)}{\tau_{cw}} - \frac{N_w}{\tau_{wr}} \quad (1)$$

$$\frac{\partial N_c}{\partial t} = \frac{N_w(1-f_c)}{\tau_{wc}} - \frac{N_c(1-f_w)}{\tau_{cw}} + \frac{N_e(1-f_c)}{\tau_{ec}} - \frac{N_c(1-f_e)}{\tau_{ce}} + \frac{N_g(1-f_c)}{\tau_{gc}} - \frac{N_c(1-f_g)}{\tau_{cg}} \quad (2)$$

$$\frac{\partial N_e}{\partial t} = \frac{N_c(1-f_e)}{\tau_{ce}} - \frac{N_e(1-f_c)}{\tau_{ec}} + \frac{N_g(1-f_e)}{\tau_{ge}} - \frac{N_e(1-f_g)}{\tau_{eg}} \quad (3)$$

$$\frac{\partial N_g}{\partial t} = \frac{N_c(1-f_g)}{\tau_{cg}} - \frac{N_g(1-f_c)}{\tau_{gc}} + \frac{N_e(1-f_g)}{\tau_{eg}} - \frac{N_g(1-f_e)}{\tau_{ge}} - \frac{N_g h_g}{\tau_{gr}} - \frac{g_m(f_g+h_g-1)P}{\sigma\hbar\omega} \quad (4)$$

where D_w, D_c , D_e and D_g are the degeneracies of the corresponding electron states, J is the injection current density, e is the electron charge, l_w is the thickness of the WL, $\hbar\omega$ is the

photon energy corresponding to the GS transition, P is the optical power, σ is the cross section of the active region, and NQ is the surface density of QDs. The effective volume density of the QDs is $\widetilde{NQ}$ given by $\widetilde{NQ} = NQ/l_w$. g_m is the maximum modal gain, which depends on the confinement factor of each QD, the surface density of QDs, and the number of QD layers. The modal gain in GS is g, given by $g_m(f_g + h_g - 1)$. The hole occupation probability in the GS in the valence band of QDs is h_g. The electron spontaneous recombination lifetimes in the WL and the GS are τ_{wr} and τ_{gr}, respectively. The electron occupation probabilities are related to the corresponding electron densities by [7]

$$N_w = 2D_w \widetilde{NQ} f_w \qquad (5a)$$

$$N_c = 2D_c \widetilde{NQ} f_c \qquad (5b)$$

$$N_e = 2D_e \widetilde{NQ} f_e \qquad (5c)$$

$$N_g = 2D_g \widetilde{NQ} f_g \qquad (5d)$$

The associated that the time constants are the electron relaxation from the wetting layer to the CS (τ_{wc}) is given by [8]

$$\tau_{wc} = \frac{\tau_{wc0}}{1 + C_{wc} f_w} \qquad (6)$$

where τ_{wc0} is the electron capture time solely associated with the phonon-assisted process, C_{wc} is the dimensionless ratio of the Auger-assisted coefficient to the phonon-assisted coefficient in the capture process. The electron escape time from the CS to the WL is τ_{cw} and can be expressed, under the condition of thermal equilibrium, by [4]

$$\tau_{cw} = \tau_{wc} \exp\left(\frac{\Delta E_{wc}}{KT}\right) \qquad (7)$$

where ΔE_{wc} is the energy separation between the WL bandedge and the CS in the conduction band of QDs, K is the Boltzmann's constant, and T is the room temperature. The same relationship is applied to the intradot relaxations and excitations thereby the intradot relaxation and excitation times in Eqs. (2)–(4) can be expressed as [9]

$$\tau_{ij} = \frac{\tau_{ij}}{1 + C_{ij} f_w} \quad i = c, e \; ; j = e, g; i \neq j \qquad (8)$$

$$\tau_{ji} = \frac{D_j}{D_i} exp\left(\frac{\Delta E_{ij}}{KT}\right) \tau_{ij} \quad i = c, e \; ; j = e, g; i \neq j \qquad (9)$$

where τ_{ij} is the phonon-dominated relaxation time and C_{ij} is the dimensionless ratioof the Auger-assisted coefficient to the phonon-assisted coefficient in the relaxation processes, and ΔE_{ij} is the energy separation between the ith state and the jth state in the conduction band of QDs.

3. Overall Charge Neutrality of QD-SOA

Most of the literature assume that the carrier dynamics is determined by the relxation of electrns in the conduction band, because of the much larger effective mass of holes and lower quantization energies of the QD levels in the valence band which results in a faster relaxation of holes. Therefore, electrons behavior limits the carrier dynamics while holes in the valence band are assumed to be in quasi-thermal equilibrium at all times. For this reason, the relaxation rates of the electron states in the conduction band and the hole states in the valence band are assumed to be the same, and only the electron rate equations are used i.e. $g = g_m(2f_g - 1)$[10]. The main contribution of the present work is investigating the effect of hole dynamics. It is considered by using the overall charge neutrality of the QD-SOA as follows [9]

$$f_g + D_e f_e + D_c f_c + D_w f_w = h_g + D_e h_e + D_c h_c + D_w h_w \qquad (10)$$

where h_w, h_c and h_e are the hole occupation probabilities in the WL bandedge, CS, and ES in the valance band of QDs, respectively. Due to the larger effective mass of holes and the resulting small separation between energy levels, holes can be assumed to be in equilibrium all times over the entire valence band. The hole occupation probabilities satisfy the Fermi–Dirac distribution and can be written as [9]

$$h_i = \frac{1}{1 + exp\left[-\left(\frac{E_i^v - E_f^v}{KT}\right)\right]} \qquad i = w, c, e, g \tag{11}$$

where E_f^v is the quasi-Fermi level of the valence band. In a traveling-wave QD-SOA.

4. Small-Signal XGM Model

In this section, an analytical model for the small-signal XGM mechanism which takes into account the hole effect is derived. It is assumed that a pump P_0 and probe P_1 signals are injected into the amplifier. The pump signal consists of a continuous wave (CW) and a small signal while the probe signal consists of only a CW signal. The interaction between the probe and the pump signal via XGM causes modulation of the probe signal. The small-signal variation of the probe signal and pump are denoted as p_1 and p_0, respectively. Assume that the occupation probabilities in WL, CS, ES and GS can be decomposed as

$$\mathbf{f}_i = f_i + \Delta f_i e^{-j\Omega t} \qquad i = w, c, e \text{ and } g \tag{12a}$$

$$\mathbf{h}_g = h_g + \Delta h_g e^{-j\Omega t} \tag{12b}$$

where h_g is the hole occupation probabilities in the GS in the valance band of QDs, , Δh_g is the induced change in the occupation probability due to XGM, f_i is the value of the occupation probability at steady-state, Δf_i is the induced change in the occupation probability due to XGM, and Ω denotes the frequency detuning between the pump and probe signals. By perturbing Eqs. (1)–(4), and assuming harmonic modulation, one can get expressions for (Δf_g), (Δf_e), (Δf_c) and (Δf_w) as follows

$$\Delta f_g = \frac{-g_m[(f_g + h_g - 1)(p_0 + p_1)]/2D_g\widetilde{N}Q\sigma\hbar\omega}{\left[\begin{array}{c} -j\Omega + \frac{\Delta f_c}{\Delta f_g}\left(\frac{D_c(f_g - 1)}{D_g\tau_{cg}} - \frac{f_g}{\tau_{gc}}\right) + \frac{g_{max}(P_0 + P_1)}{2D_g\widetilde{N}Q\sigma\hbar\omega} \\ + \left(\frac{D_c f_c}{D_g\tau_{cg}} + \frac{(1 - f_c)}{\tau_{gc}}\right) + \frac{\Delta f_e}{\Delta f_g}\left(\frac{D_e(f_g - 1)}{D_g\tau_{eg}} - \frac{f_g}{\tau_{ge}}\right) \\ + \frac{\Delta h_g}{\Delta f_g}\left(\frac{(g_{max}(P_0 + P_1))}{2D_g\widetilde{N}Q\sigma\hbar\omega} + \frac{f_g}{\tau_{gr}}\right) + \frac{h_g}{\tau_{gr}} + \frac{D_e f_e}{D_g\tau_{eg}} \\ + \frac{(1 - f_e)}{\tau_{ge}} \end{array}\right]} \tag{13}$$

$$\frac{\Delta f_e}{\Delta f_g} = \frac{\frac{\Delta f_c}{\Delta f_g}\left(\frac{D_c(1 - f_e)}{D_e\tau_{ce}} + \frac{f_e}{\tau_{ce}}\right) + \frac{D_g(1 - f_e)}{D_e\tau_{ge}} + \frac{f_c}{\tau_{eg}}}{-j\Omega + \frac{D_c f_c}{D_e\tau_{ce}} + \frac{(1 - f_c)}{\tau_{ec}} + \frac{D_g f_g}{D_e\tau_{ge}} + \frac{(1 - f_g)}{\tau_{eg}}} \tag{14}$$

$$\frac{\Delta f_c}{\Delta f_g} = \frac{\left(\frac{D_g(1 - f_c)}{D_c\tau_{gc}} + \frac{f_c}{\tau_{cg}}\right) + \frac{A\left(\frac{D_g(1 - f_e)}{D_e\tau_{ge}} + \frac{f_c}{\tau_{eg}}\right)}{B}}{\left[\begin{array}{c} -j\Omega + \frac{D_w f_w}{D_c\tau_{wc}} + \frac{(1 - f_w)}{\tau_{cw}} + \frac{D_e f_e}{D_c\tau_{ec}} \\ + \frac{(1 - f_e)}{\tau_{ce}} + \frac{D_g f_g}{D_c\tau_{gc}} + \frac{(1 - f_g)}{\tau_{cg}} \\ -C\left(\frac{\left(\frac{f_w}{\tau_{wc}} + \frac{D_c(1 - f_w)}{D_w\tau_{cw}}\right)}{-j\Omega + \frac{(1 - f_c)}{\tau_{wc}} + \frac{D_c f_c}{D_w\tau_{cw}} + \frac{1}{\tau_{wr}}}\right) \\ - \frac{A\left(\frac{D_c(1 - f_e)}{D_e\tau_{ce}} + \frac{f_e}{\tau_{ec}}\right)}{B} \end{array}\right]} \tag{15}$$

Where

$$A = \left(\frac{D_e(1 - f_c)}{D_c\tau_{ec}} + \frac{f_c}{\tau_{ce}}\right)$$

$$B = -j\Omega + \frac{D_c f_c}{D_e\tau_{ce}} + \frac{(1 - f_c)}{\tau_{ec}} + \frac{D_g f_g}{D_e\tau_{ge}} + \frac{(1 - f_g)}{\tau_{eg}}$$

$$C = \left(\frac{D_w(1 - f_c)}{D_c\tau_{wc}} + \frac{f_c}{\tau_{cw}}\right)$$

The contribution in this paper is the hole effect, it is given by using eqs. (11-12) as follow

$$\frac{\Delta h_g}{\Delta f_g} = \frac{D_g + D_e\frac{\Delta f_e}{\Delta f_g} + D_c\frac{\Delta f_c}{\Delta f_g} + D_w\frac{\Delta f_w}{\Delta f_g}}{8.1368} \tag{16}$$

Where

$$\frac{\Delta f_w}{\Delta f_c} = \left(\frac{\left(\frac{f_w}{\tau_{wc}} + \frac{D_c(1 - f_w)}{D_w\tau_{cw}}\right)}{-j\Omega + \frac{(1 - f_c)}{\tau_{wc}} + \frac{D_c f_c}{D_w\tau_{cw}} + \frac{1}{\tau_{wr}}}\right) \tag{17}$$

The rate equations for $\mathbf{P}_0$ **and** $\mathbf{P}_1$, and the rate equations for the small signals p_0 and p_1 are given by

$$\frac{d\mathbf{P}_0}{d\mathbf{z}} = (\mathbf{g}_m(\mathbf{f}_g + \mathbf{h}_g - 1) - \alpha)\mathbf{P}_0 \tag{18a}$$

$$\frac{\partial \mathbf{p}_0}{\partial \mathbf{z}} = \mathbf{g}_m(\mathbf{f}_g + \mathbf{h}_g - 1)[(1 - \alpha)\mathbf{p}_0 - 2\mathbf{g}_m\psi_{TCDD}(\mathbf{p}_0 + \mathbf{p}_1)(\mathbf{P}_0 + \mathbf{p}_0)] \tag{18b}$$

IJSER

$$\frac{dP_1}{dz} = (g_m(f_g + h_g - 1) - \alpha)P_1 \quad \textbf{(18c)}$$

$$\frac{\partial p_1}{\partial z} = g_m(f_g + h_g - 1)[(1-\alpha)p_1 - 2g_m\psi_{TCDD}(p_0 + p_1)(P_0 + p_0)] \quad \textbf{(18d)}$$

Where

$$\psi_{TCDD} = \frac{1/2D_g\widetilde{N}Q\sigma\hbar\omega}{j\Omega + \frac{\Delta f_c}{\Delta f_g}\left(\frac{D_c(f_g-1)}{D_g\tau_{cg}} - \frac{f_g}{\tau_{gc}}\right) + \frac{D_cf_c}{D_g\tau_{cg}} + \frac{(1-f_c)}{\tau_{gc}} + \frac{\Delta f_e}{\Delta f_g}\left(\frac{D_e(f_g-1)}{D_g\tau_{eg}} - \frac{f_g}{\tau_{ge}}\right) + \frac{h_g}{\tau_{gr}} + \frac{(1-f_e)}{\tau_{ge}} + \frac{g_{max}(P_0+P_1)}{2D_g\widetilde{N}Q\sigma\hbar\omega} + \frac{D_ef_e}{D_g\tau_{eg}} + \frac{\Delta h_g}{\Delta f_g}\left(\frac{(g_{max}(P_0+P_1))}{2D_g\widetilde{N}Q\sigma\hbar\omega} + \frac{f_g}{\tau_{gr}}\right)} \quad \textbf{(19)}$$

When an ideal facet reflectivity is assumed and the effect of amplified spontaneos emission is not included for simplicity. The small-signal cross gain modulation efficiency is calculated as [40]

$$\eta = (P_0(0)/P(0))(1 - exp(-F)) \quad \textbf{(20)}$$

Where

$$F = ln\left(\frac{-j\Omega + \tau_{eff}^{-1}(\Omega) + 2aP(L)}{-j\Omega + \tau_{eff}^{-1}(\Omega) + 2aP(0)}\right) \quad \textbf{(21)}$$

Where

$$\tau_{eff}(\Omega) = \frac{1/2D_g\widetilde{N}Q\sigma\hbar\omega}{\left[\frac{\Delta f_c}{\Delta f_g}\left(\frac{D_c(f_g-1)}{D_g\tau_{cg}} - \frac{f_g}{\tau_{gc}}\right) + \frac{\Delta f_e}{\Delta f_g}\left(\frac{D_e(f_g-1)}{D_g\tau_{eg}} - \frac{f_g}{\tau_{ge}}\right) + \frac{\Delta h_g}{\Delta f_g}\left(\frac{(g_{max}(P_0+P_1))}{2D_g\widetilde{N}Q\sigma\hbar\omega} + \frac{f_g}{\tau_{gr}}\right) + \left(\frac{D_cf_c}{D_g\tau_{cg}} + \frac{(1-f_c)}{\tau_{gc}}\right) + \left(\frac{D_ef_e}{D_g\tau_{eg}} + \frac{(1-f_e)}{\tau_{ge}} + \frac{h_g}{\tau_{gr}}\right)\right]} \quad \textbf{(22)}$$

5. Results and Discussion

The values of the parameters used in modeling the QD-SOA are [9,11-12] : NQ = 5×10^{10} cm^{-2}, α_{loss} = 3 cm^{-1}, g_m = 19.5 cm^{-1}, l_w = 2×10^{-5} cm, σ = 2.5×10^{-6} cm^2, L=0.33 cm, τ_{ce0}=10 ps, τ_{eg0}=10 ps, τ_{cg0}= 10 ps, τ_{wc0}= 1 ps, τ_{wr}= 1 ns, τ_{gr}=1 ns, m_h^* = 0.0742 m_e kg, m_e^* = 0.026 m_e kg, C_{ce} = 50, C_{wc} = 0.25, C_{cg} = 25, C_{eg} = 50, D_c = 10, D_e =3, D_g = 1, D_W = 250, ΔE_{wc}^C=134.56 mev, ΔE_{ce}^C= 111.07 mev, ΔE_{eg}^C=51.836 mev, ΔE_{wc}^V=46.706 mev, ΔE_{ce}^V=38.922 mev, ΔE_{eg}^V= 18.163 mev. Equations (18a)-(18d) are solved numerically using fourth-order Runge-Kutta method with the following boundary conditions: $P_0 = 0.05\ P_{sat0}, P_1 = 0.1\ P_{sat0}, p_0 = 0.1\ P_0, p_1 = 0$. The value of P_{sat0} is estimated to be 50 mW for the amplifier under consideration. XGM however, has three different physical mechanisms namely spectral-hole burning (SHB), carrier heating (CH) and total carrier density depletion (TCDD). The dominant gain saturation mechanism of QD SOAs can be select depending on the values of injection current density, signal power, and modulation frequency. At small values of the injection current density, signal power and the modulation frequency, the dominant XGM mechanism becomes TCDD. This is necessary to investigate the efficiency of present model. Fig. 1 shows the variation of the small-signal XGM response with detuning modulation frequency for the intersubband carrier relaxation time from the ES to GS ($\tau_{eg} = 1ps$) when charge neutrality for whole device and charge neutrality in GS only are assumed. The other relaxation/escape lifetimes are assumed to be constant.

Fig.1: calculated small-signal XGM response when the

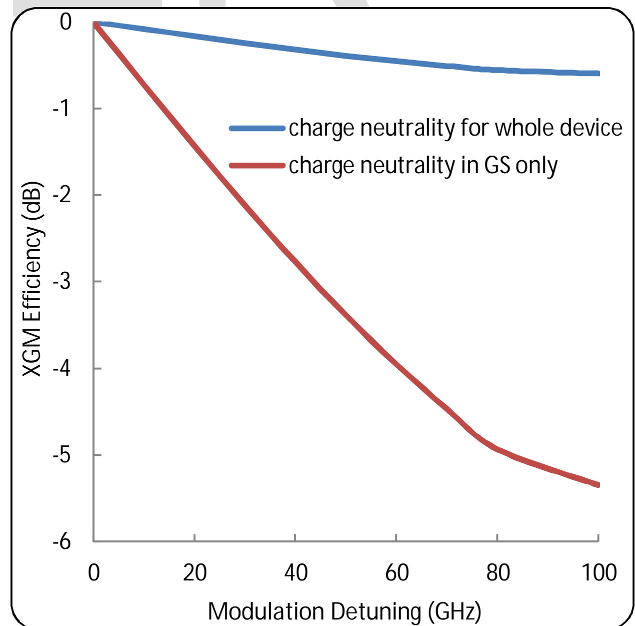

intersubband carrier relaxation time from ES to GS ($\tau_{eg} = 1ps$).

It is clear that, the fast intersubband carrier relaxation time gives a better small-signal 3-dB XGM bandwidth for charge

neutrality for whole device case. This result comes from the fact that the change in both hole and electron occupation leads to change in gain value..

Fig. 2 shows the calculated small-signal XGM responses for charge neutrality for whole device and charge neutrality in GS only when the intersubband carrier relaxation time from the CS to GS (τ_{cg} = 1ps) and the other

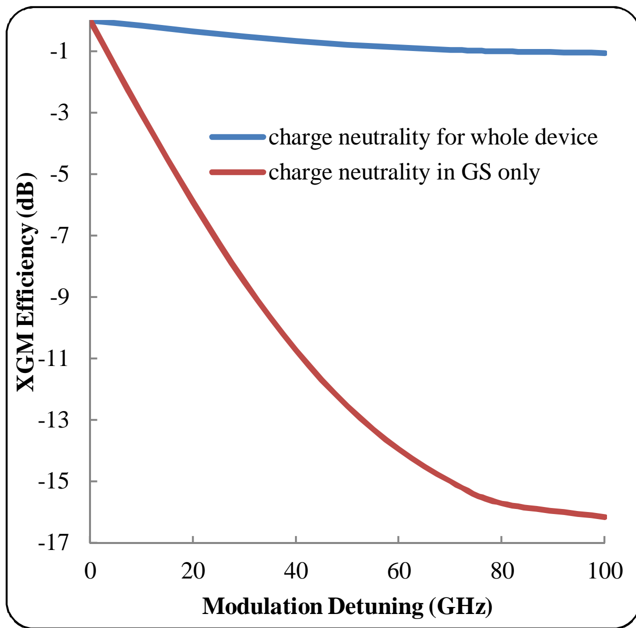

relaxation/escape lifetimes are assumed to be constant.

Fig.2: Calculated small-signal XGM response when the intersubband carrier relaxation time from the ES to GS (τ_{cg} = 1ps).

It is clear that, the charge neutrality for whole device gives a better small-signal 3-dB XGM bandwidth the faster injecting of carriers from carrier reservoirs CS to GS significantly enhances XGM induced by TCDD, and improves the high-speed XGM response at the GS. On the other hand, the faster injecting of carriers to carrier reservoirs such as CS and ES significantly enhances XGM induced by SHB.

Fig. 3 shows the variation of small-signal XGM responses for charge neutrality for whole device and charge neutrality in GS only when the intersubband carrier relaxation time from the WL to CS (τ_{wc} = 3ps) and the other relaxation/escape lifetimes are assumed to be constant. It is clear that, the calculated small-signal XGM response continues to decrease as the modulation frequency increases. At low injection current, the QD carrier reservoirs such as the WL and CS are nearly empty and the dominant XGM mechanism becomes TCDD. When the injection current is high, the QD carrier reservoirs

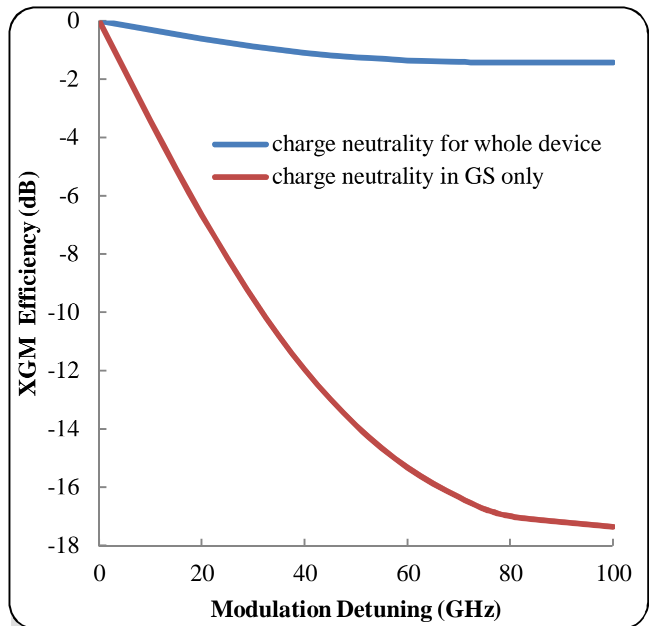

are fully occupied and SHB becomes the dominant XGM mechanism.

Fig.3. calculated small-signal XGM response when the intersubband carrier relaxiation time from the WL to CS (τ_{wc} = 3ps).

Fig. 4 shows the variation of the small-signal XGM response with detuning modulation frequency for the intersubband carrier relaxation time from the CS to ES (τ_{ce} = 10ps) when charge neutrality for whole device and charge neutrality in GS only are assumed. The other relaxation/escape lifetimes are assumed to be constant.

At low modulation frequencies, the XGM due to TCDD is dominant. On the contrary, at high modulation frequencies, the XGM due to SHB becomes significant. Therefore, the improvement of the measured small-signal XGM responses at low injection current is ascribed to the enhanced XGM due to TCDD

by means of injected carriers from the QD carrier reservoirs such as the ES.

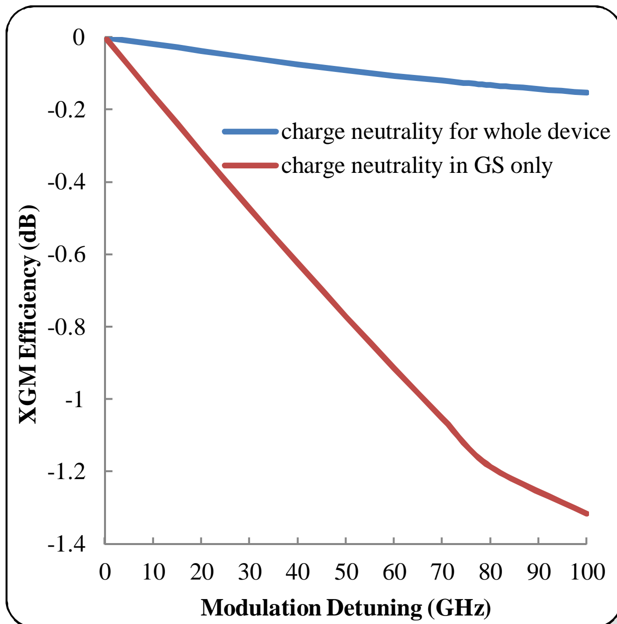

Fig. 4: Calculated small-signal XGM response when the intersubband carrier relaxation time from the CS to ES ($\tau_{ce} = 10ps$).

6. Conclusions

XGM wavelength conversion in QD-SOA are studied taking into account the effect of hole dynamics. Based on four-level rate equation model (4LREM) preserving charge neutrality for quantum-dot semiconductor optical amplifiers (QD-SOAs) an analytical model is derived to investigate the XGM responses in the saturation regime. Charge neutrality in GS only is assumed for mathematical simplicity. But, the Charge neutrality for whole device case, gives a accurate and better small-signal 3-dB XGM bandwidth in comparison with that of the Charge neutrality in GS only because the calculation of the change in hole occupation leads to get the accurate gain change.

7. References

[1] R. Ramaswami and K. N. Sivarajan, *Optical Networks*, Second ed. New York: Academic Press, 2002.

[2] I. Glesk, B. C.Wang, L. Xu, V. Baby, and P. R. Prucnal, “Ultrafast alloptical switching in optical networks,” in *Progress in Optics*, E. Wolf, Ed. New York: Elsevier, 2003, vol. 45, pp. 53–117.

[3] D. Bimberg, M. Grundmann, and N. N. Ledentsov, *Quantum Dot Heterostructures*. New York: Wiley, 1999.

[4] G. P. Agrawal, *Fiber Optic Communication Systems*, 3rd ed. New York: Wiley, 2002.

[5] C. Z. Tong, S. F. Yoon, C. Y. Ngo, C. Y. Liu, and W. K. Loke, “Rate equations for 1.3-µm dots-under-a-well and dots-in-a-well self-assembled InAs-GaAs quantum-dot lasers,” IEEE J. Quantum Electron, vol. 42, no. 11, pp. 1175–1183, Nov. 2006.

[6] J. Xiao and Y. Huang, “Numerical analysis of gain saturation, noise figure, and carrier distribution for quantum-dot semiconductor-optical amplifiers,” IEEE J. Quantum Electron., vol. 44, no. 5, pp. 448–455, May 2008.

[7] J. Kim and S. L. Chuang, “Small-signal cross-gain modulation of quantum-dot semiconductor optical amplifiers ,” IEEE Photon. Technol. Lett., vol. 18, no. 23, pp. 2538–2540, Dec.2006.

[8] T. W. Berg and J. Mørk, “Saturation and noise properties of quantum-dot optical amplifiers,” IEEE J. Quantum Electron., vol. 40, no. 11, pp. 1527–1539, Nov. 2004.

[9] X. Li and G. Li, “Static Gain, Optical Modulation Response, and Nonlinear Phase Noise in Saturated Quantum-Dot Semiconductor Optical Amplifiers”,” IEEE J. Quantum Electron, vol. 45, no.5, 499–505 May, 2009.

[10] M. Sugawara, H. Ebe, N. Hatori, M. Ishida, Y. Arakawa, T. Akiyama, K. Otsubo, and Y. Nakata, “Theory of optical signal amplification and processing by quantum-dot semiconductor optical amplifiers,” Phys. Rev., vol. B69, pp. 235332-1–39, 2004.

[11] J. T. Verdeyen , Laser electronics ,(Prentice-Hall, New Jersey 1995)

[12] M. Sugawara, T. Akiyama, N. Hatori, Y. Nakata, H. Ebe, and H. Ishikawa, “Quantum-dot semiconductor optical amplifiers for high-bit-rate signal processing up to 160 Gbs^{-1} and a new scheme of 3R regenerators,” Meas. Sci. Technol., vol. 13, pp. 1683–1691, 2002.

IJSER